Three-Phase Contact Line Energetics from Nanoscale Liquid Surface Topographies

T. Pompe[1] and S. Herminghaus[2,*]

[1]*Max-Planck-Institut für Kolloid- und Grenzflächenforschung, 14424 Potsdam, Germany*
[2]*Universität Ulm, Abteilung Angewandte Physik, Albert-Einstein-Allee 11, 89069 Ulm, Germany*

(Received 23 December 1999)

The contact line tension of a three-phase system (solid-liquid-vapor) is determined from the liquid surface topography data obtained with scanning force microscopy. The data are analyzed in two completely complementary ways, one of which is based on the modified Young equation, the other on the effective interface potential derived from the profile of the liquid-vapor interface in the three-phase region. The two methods agree quite well for the systems investigated. Contact line tensions are in the range of 10^{-11} to 10^{-10} J/m, which is consistent with theory.

PACS numbers: 81.30.Dz, 68.45.–v

The contact line tension (CLT), i.e., the excess free energy of a solid-liquid-vapor system per unit length of the contact line, is probably the most controversial quantity in wetting science. Because of its very small value—theory predicts that τ be on the order of some 10^{-11} J/m [1–5]—quantitative measurements are difficult and a large scatter of experimental values was obtained, ranging from 10^{-12} to 10^{-5} J/m [6–10]. The main reason is the limited resolution of the microscopy techniques used. A characteristic length scale for the influence of the CLT, τ, can be estimated by relating a typical value expected for τ to a typical interface tension σ, which yields $\tau/\sigma = 10^{-11}$ J/m/10^{-2} J/m^2 = 1 nm. In other words, a measurable influence of the CLT is to be expected in the nanometer range, while on larger scales, interfacial tension will dominate the system. Consequently, inherent to low resolution techniques such as optical microscopy there is considerable coarse graining resulting in an "effective" CLT, which may be largely determined, e.g., by the interplay between interfacial tension and nanoscale substrate inhomogeneity.

In order to overcome these problems, we used scanning force microscopy (SFM) in tapping mode to image the topography of liquid sessile droplets. This was recently shown to give quantitatively reliable results with a spatial resolution of a few nanometers [11,12]. Once the liquid topography close to the three-phase contact line is known, it is straightforward to derive the CLT from these data, which can be done in two complementary ways. The first approach, which we call the contact angle approach, proceeds along the lines of the modified Young equation [13,14]

$$\cos(\Theta) = \cos(\Theta_{\mathrm{Young}}) - \frac{1}{\sigma}\tau\kappa\,, \qquad (1)$$

where Θ is the actual contact angle the droplet forms with the substrate, and Θ_{Young} is the contact angle according to the Young equation for a straight contact line, or an infinitely large drop. κ is the curvature of the contact line, and σ is the surface tension of the liquid. From Eq. (1), a linear dependence of the cosine of the local contact angle upon the local curvature of the contact line is expected. Experimental determination of Θ for various curvatures, κ, thus allows one to derive the CLT.

In order to create liquid surface topographies with high contact line curvatures, substrates with an artificial striped wettability pattern were prepared. This was done by microcontact printing [15–17] of perfluorinated alkylsilanes [(heptadecafluoro-1,1,2,2-tetrahydrodecyl)dimethylchlorosilane; ABCR, Germany] onto hydrophilic silicon wafers (Wacker Siltronics, Germany) with a native oxide layer. A stripewise wettability contrast of hydrophobic and hydrophilic domains with a periodicity between 200 and 1000 nm was obtained. This technique minimizes the possible influence of topography effects since the roughness of the silicon wafer (2–3 Å) as well as the height of the stamped alkylsilane monolayers (<1 nm) are negligible. The details of this preparation procedure and its pitfalls are described elsewhere [18]. The liquid topographies were obtained with Nanoscope IIIa and Dimension 3000 (Digital Instruments, USA) SFMs. Commercially available silicon cantilevers were used as supplied, with resonance frequencies around 300 kHz (Pointprobe™, Si–cantilever; Nanoprobe, Germany).

When a micron sized liquid droplet is deposited from the aerosol phase onto the prepared wettability structure of the substrate, the liquid arranges into its equilibrium shape determined by the different interface energies of the hydrophobic and hydrophilic stripes of the substrate. Effects of contact angle hysteresis, such as changes in contact angle during gradual evaporation of the droplets, have not been observed. Figure 1 shows a three-dimensional SFM topography closeup of a water droplet contact line. It exhibits a typical structure comprising regions of high contact angle on the hydrophobic stripes and regions of lower contact angle on the hydrophilic stripes, together with a pronounced curvature of the contact line. From sections through the topographic images taken perpendicular to the contact line at the point of interest, it is possible to determine the local contact angle as well as the local contact line curvature along the contact line [17]. Care must be taken

 0031-9007/00/85(9)/1930(4)$15.00

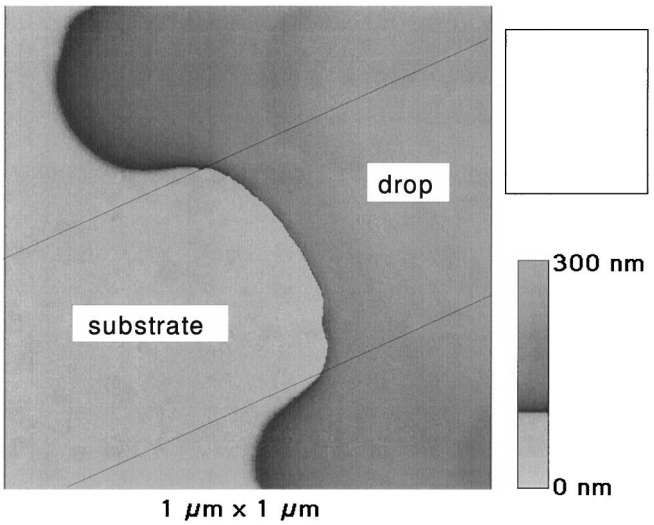

FIG. 1. SFM topography image (top view, 1 μm $\times$ 1 μm) of the contact line region of a water droplet on a silicon wafer with stripewise patterned wettability. The dashed lines indicate the boundaries of a hydrophobic domain. The strong corrugation of the contact line induced by the wettability pattern allows the measurement of the dependence of the local contact angle upon the contact line curvature.

to exclude from the fit those parts of the profile which are close enough to the surface to be affected by the long-range wetting forces (see below).

The cosine of the contact angle is plotted versus the contact line curvature in Fig. 2 for a hexaethylene glycol droplet ($\sigma = 45$ mN/m) [19]. For high contact angles [small $\cos(\Theta)$], a linear dependence of $\cos(\Theta)$ upon κ is observed, from which a CLT of $\tau = -3 \times 10^{-10}$ J/m can be derived. In the region of low contact angles, a linear dependence of $\cos(\Theta)$ upon κ is found as well and $\tau = -1 \times 10^{-10}$ J/m is obtained there. Data points with an intermediate contact angle do not exhibit a clear dependence between $\cos(\Theta)$ and κ. It corresponds to that part of the contact line which is close to the domain boundary of the hydrophobic and hydrophilic stripes on the substrate. In this region, the CLT effect interferes with effects of imperfections of the lateral change of the surface energy. It should be stressed that our results for the CLT are in the range of $\approx 10^{-11}$ J/m as predicted from theory, in contrast to values up to 10^{-5} J/m as measured in other experiments [6,9].

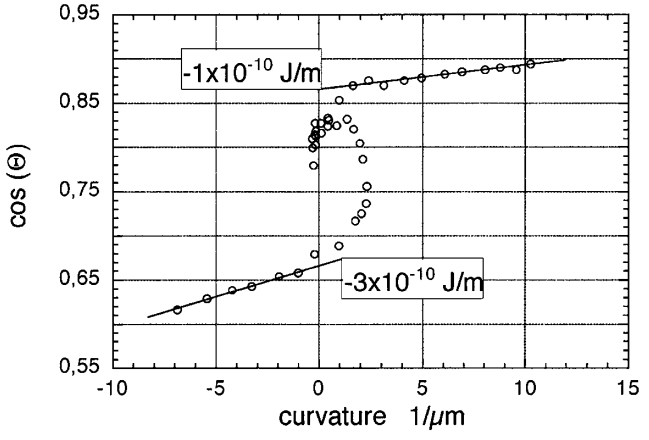

FIG. 2. The cosine of the local contact angle is plotted versus the local curvature of the contact line, κ, for a hexaethylene glycol droplet sitting on a patterned silicon wafer (cf. Fig. 1). On both the hydrophobic and hydrophilic domains of the substrate, a linear dependence is observed, yielding a CLT of $\tau = -3 \times 10^{-10}$ J/m and $\tau = -1 \times 10^{-10}$ J/m, respectively. Intermediate values of $\cos(\Theta)$ stem from the boundary regions and are thus not well defined.

Moreover, due to the very high resolution of SFM, it is possible to use a second, complementary approach to determine the CLT, which will be called the interface potential approach. It makes use of the effective interface potential ω of the system, which can be obtained in a straightforward manner from the liquid surface topography. Figure 3 shows the profiles $l(x)$ of the vapor-liquid interface near the surface of the solid substrate measured by SFM for three different systems. In order to avoid artifacts from the global liquid surface topography, it is essential to measure these profiles at places where the contact line has negligible curvature. These can always be found due to the characteristic faceting of the droplets [20].

The lateral scale in Fig. 3 is normalized such as to equalize the slope of the profiles for the asymptotic behavior far away from the substrate. The straight line is what one would expect, if there was no finite-range contribution in the effective interface potential. The deviation of the measured profiles from this line allows one to calculate the

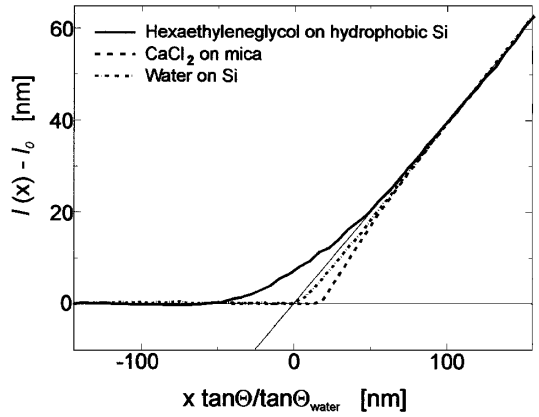

FIG. 3. Vapor-liquid interface profiles $l(x)$ measured by SFM of the three-phase region of the three different systems investigated. The lateral scale is normalized to equalize the asymptotic behavior far away from the substrate surface. Thus, all three profiles of hexaethylene glycol on hydrophobized silicon wafer (—·—, $\Theta = 55°$), aqueous $CaCl_2$ solution on mica (— — —, $\Theta = 5.5°$), and water on silicon wafer (– – –, $\Theta = 21°$) together with the straight solid lines [$a(x)$] corresponding to the absence of finite-range interactions (———) have the same slope in the plot for large values of $l(x)$. One can clearly see the deviations of the profiles from the straight line due to the different three-phase interaction.

free energy contribution of the three-phase interaction in the contact region. From the fact that these deviations are different (even of different sign) for the various systems studied demonstrates that they are not to be assigned to artifacts due to the imaging process.

The CLT, τ, can be obtained by integration of the effective interface potential. From the Euler-Lagrange equation [1,21] for the profile $l(x)$, we obtain

$$\omega(l(x)) = \sigma\left\{\cos\Theta - \frac{1}{\sqrt{1 + l'^2(x)}}\right\}. \qquad (2)$$

It should be noted in passing that the surface tension may be different from its value at the free surface of the bulk liquid when $l(x)$ becomes as small as the bulk correlation length. However, since our experiments were performed far from the critical points of all of the substances involved, these effects have been neglected here. Consequently, σ is considered constant. With the effective interface potential at hand, as obtained from Eq. (2), it is straightforward to calculate the CLT. It mainly consists of two contributions [1,21], $\tau = \tau_\omega + \tau_i$. The first one, τ_ω, is the integral over $\omega(l)$ and the second one, τ_i, is the contribution of the additional vapor-liquid interface, which arises due to the fact that one deals not with a liquid film on a solid substrate having two parallel interfaces, but with a profile of laterally varying slope. To a very good approximation [1], one obtains

$$\tau_\omega = \int_{-\infty}^{+\infty} \{\omega(l(x)) - \omega(a(x))\}\, dx + \frac{1}{\tan\Theta} \int_{l_0}^{+\infty} \omega(l)\, dl \qquad (3)$$

and

$$\tau_i = \sigma \int_{-\infty}^{+\infty} \{\sqrt{1 + l'(x)^2} - \sqrt{1 + a'(x)^2}\}\, dx \qquad (4)$$

where l_0 is the equilibrium film thickness away from the drop, which is usually of the order of a molecular layer. The function $a(x) := H(-x)l_0 + H(x)x\tan\Theta$ (where H is the Heaviside step function) describes the asymptotic behavior of the profile as indicated by the thin solid lines in Fig. 3. The x coordinate is chosen so as to assign $x = 0$ to the intersection of the lines. Based on the above equations, measurement of $l(x)$ with SFM allows one for the first time to directly calculate $\omega(l)$ and τ from the experiment.

To compare the results of the interface potential approach with those from the contact angle approach, all measured values of the CLT, determined with both approaches, are summarized in Table I. The values scatter in a range of 20% to 50% of the measured quantity. By deconvolution of the influence of the size of the SFM tip on the measured profiles $l(x)$, it could be verified that this effect is negligible compared to the experimental scattering of the data. In particular, a finite tip radius of 20 nm would result in a decrease of the measured CLT (as determined by the interface potential approach) of less than 10%. Since our tips had radii of 5 to 10 nm (as specified by the manufacturer), it is clear that the errors in the measurement are dominated by other sources, such as scattering of the data.

We see that all values are in the range of 10^{-11} to 10^{-10} J/m, as expected from theory. Depending on the system investigated, positive or negative values for the CLT are found. This is in agreement with the qualitatively different three-phase interactions of the systems investigated. Furthermore, the values obtained from the two different approaches agree quite well with each other, although they are based on a different theoretical background. The contact angle approach uses the large scale model of the Young equation with constant interface energies. Only as a first order perturbation the three-phase interaction is included in the modified Young equation, with the basic assumption that the region of the three-phase interaction is more or less one-dimensional. Thus, the CLT is derived from its effective influence on the mesoscopic parameters of this model, the contact angle, and the contact line curvature. In contrast, the interface potential approach is based on the detailed structure of the three-phase region. Direct information about the three-phase interaction is derived, and the CLT is calculated as the free energy contribution of the three-phase interaction. The fact that these complementary approaches yield very similar results gives us the confidence that the values obtained are, within the still considerable experimental errors, quite reliable.

Helpful discussions with S. Dietrich, C. Bauer, J. Indekeu, and H. Dobbs are gratefully acknowledged. This

TABLE I. The CLT, τ, in units of J/m. Experimental results with the contact angle approach as well as the interface potential approach are presented for three different liquids (hexaethylene glycol, aqueous $CaCl_2$ solution, and water) on a silicon wafer surface with a stripewise wettability pattern. The values obtained with the two approaches of data analysis agree quite well. The errors correspond to the scattering of the data used in the analyses.

Liquid	Hexaethylene glycol		Aqueous $CaCl_2$ solution		Water
Substrate	Hydrophobic	Hydrophilic	Hydrophobic	Hydrophilic	Hydrophilic
Contact angle	$-3(\pm1) \times 10^{-10}$	$-1.0(\pm0.3) \times 10^{-10}$	⋯	$2.0(\pm6) \times 10^{-10}$	$7.0(\pm0.3) \times 10^{-11}$
Interface potential	$-2.0(\pm0.5) \times 10^{-10}$	$-1.0(\pm0.3) \times 10^{-10}$	$2(\pm1) \times 10^{-10}$	$1.0(\pm0.5) \times 10^{-10}$	$8(\pm2) \times 10^{-11}$

work was supported by the Deutsche Forschungsgemeinschaft within the priority program "Wetting and Structure Formation at Interfaces."

*To whom correspondence should be addressed.
Electronic address:
stephan.herminghaus@physik.uni-ulm.de

[1] T. Getta and S. Dietrich, Phys. Rev. E **57**, 655 (1998).
[2] W. D. Harkins, J. Chem. Phys. **5**, 135 (1937).
[3] F. Bresme and N. Quirke, Phys. Rev. Lett. **80**, 3791 (1998).
[4] J. S. Rowlinson and B. Widom, *Molecular Theory of Capillarity* (Oxford University Press, New York, 1984), p. 240.
[5] N. V. Churaev, V. M. Starov, and B. V. Derjaguin, J. Colloid Interface Sci. **89**, 16 (1982).
[6] D. Li and A. W. Neumann, Colloids Surf. **43**, 195 (1990).
[7] J. Drelich, J. L. Wilbur, J. D. Miller, and G. M. Whitesides, Langmuir **12**, 1913 (1996).
[8] J. Drelich, Pol. J. Chem. **71**, 525 (1997).
[9] A. Amirfazli, D. Y. Kwok, J. Gaydos, and A. W. Neumann, J. Colloid Interface Sci. **205**, 1 (1998).
[10] J. Y. Wang, S. Betelu, and B. M. Law, Phys. Rev. Lett. **83**, 3677 (1999).
[11] S. Herminghaus, A. Fery, and D. Reim, Ultramicroscopy **69**, 211 (1997).
[12] A. Fery, T. Pompe, and S. Herminghaus, J. Adhes. Sci. Technol. **13**, 1071 (1999).
[13] B. A. Pethica, Rep. Prog. Appl. Chem. **46**, 14 (1961).
[14] L. Boruvka and A. W. Neumann, J. Chem. Phys. **66**, 5464 (1977).
[15] P. F. Nealey, A. J. Black, J. L. Wilbur, and G. M. Whitesides, in *Molecular Electronics,* edited by J. Jortner and M. Ratner (Blackwell Science, Oxford, 1997), pp. 343–367.
[16] A. R. Bishop and R. G. Nuzzo, Curr. Opin. Colloid Interface Sci. **1**, 127 (1996).
[17] T. Pompe, A. Fery, and S. Herminghaus, J. Adhes. Sci. Technol. **13**, 1155 (1999).
[18] T. Pompe, A. Fery, S. Herminghaus, A. Kriele, H. Lorenz, and J. P. Kotthaus, Langmuir **15**, 2398 (1999).
[19] The considerable noise reduction with respect to the data presented in Ref. [17] is mainly due to the smaller scan range (higher spatial resolution).
[20] S. Herminghaus *et al.,* J. Phys. Condensed Matter **12**, 57 (2000).
[21] C. Bauer and S. Dietrich, Eur. Phys. J. B **10**, 767 (1999).